CONF-810684--51

LA-UR-81-3024

TITLE: RADIOGRAPHIC STUDY OF IMPACT IN POLYMER-BONDED EXPLOSIVES

AUTHOR(S): Erik Fuegiso, Q-13
J. D. Jacobson, M-4
Robert R. Karpp, M-4
Russ Jensen, Hercules Corporation, Magna, Utah

MASTER

SUBMITTED TO: Conference on Shock Waves in Condensed Media
American Physical Society
(Publication)

University of California

LOS ALAMOS SCIENTIFIC LABORATORY
Post Office Box 1663 Los Alamos, New Mexico 87545
An Affirmative Action Equal Opportunity Employer

Form No. 836 R3
St. No. 2629
12/78

UNITED STATES
DEPARTMENT OF ENERGY
CONTRACT W-7405-ENG-36

RADIOGRAPHIC STUDY OF IMPACT IN POLYMER-BONDED EXPLOSIVES*

Erik Fugelso
Jack D. Jacobson
Robert R. Karpp
Los Alamos National Laboratory
University of California

Kurt Jenser
Hercules Corporation

*Work performed under contract W-7405-ENG-36

RADIOGRAPHIC STUDY OF IMPACT IN POLYMER-BONDED EXPLOSIVES*

by

Erik Fugelso, J. D. Jacobson, Robert R. Karpp,** and Russ Jensen***

ABSTRACT

Computer-tomography generated material-density maps from flash x-ray radiographs of the impact of cylinders of mockup polymer-bonded explosive (PBX) striking a steel plate. Comparison of the density fields with computer simulation allowed discrimination of rather complex deformation and flow models for insensitive explosives to be used in further studies of chemical reactions initiated by shock waves.

An initial step to determine the mechanism of detonation initiation in the ballistic impact of insensitive high explosives is the measurement and computational modeling of the mechanical deformation. To this end, impact parameters of mockup Polymer Bonded Explosives (PBX) cylinders striking a steel plate were measured through the axisymmetric adaptation of computer assisted tomography (CAT) and compared with several numerical simulations involving different models of the PBX. CAT generates a density map throughout the cylinder at selected time intervals from low energy ray radiographs.[1,2] Features such as shock fronts, cracks and recompression zones are identified and quantified. Variations in the mathematical modelling to match early and late time behavior are somewhat complex and lead to improved characterization of the PBX mechanical models, to which reactive descriptions can later be applied.

Two flash radiographs from a set of radiographs of the impact of an inert PBX mockup on a steel plate were selected for study. The projectile was a

*Work performed under contract W-7405-ENG-36

**Los Alamos National Laboratory, Los Alamos, NM

***Hercules Corporation, Magna, Utah

right circular cylinder 8.85 mm radius, L/D ≈1.2, the impact velocity was 677 m/s. The composition of the cylinder is listed in the table. The x-ray source was 150 kev; radiographic times after initial contact with the steel plate were 4.8 and 11.2 μs.

The transmitted intensity, of an x-ray beam through the projectile is related to the incident intensity, I_0, of the x-ray from the source,

$$I = I_0 \left(\int_0^{\infty} s(e) \exp\left[-\int_0^{L} \rho(\xi) \mu(e, \xi) d\xi \right] de \right) / \left(\int_0^{\infty} s(e) de \right) \qquad (1)$$

where $\rho(\xi)$ is the material density, $\mu(e, \xi)$ is the x-ray absorption coefficient, which is a function of x-ray energy, e, s(e) is the distribution function of the energy of the x-ray source and ξ is the path of the x-ray.

Equation (1) reduces to a simple exponential if either μ is independent of the x-ray energy or the x-ray source is monochromatic. If the absorption coefficient is not independent of the x-ray energy and the source is not monochromatic radiation, it is possible to calculate an effective constant absorption coefficient through a nonlinear stretching transformation, utilizing the property that the transmitted intensity decreases monotonically with increasing thickness.

In either case the intensity can be written in a simpler form,

$$\ln I = \left(-\int \rho \mu d\xi \right) + \ln I_0 \quad . \qquad (2)$$

The negative logarithm of the x-ray intensity, after corrections for nonuniform incident intensity and geometric beam spreading is proportional to the integral of the product of the material density and the x-ray absorption coefficient. The projile has axisymmetry and, if we select values of this integral on a plane slice perpendicular to the axis of symmetry, elementary application of the techniques of computer assisted tomography will allow reconstruction of the material density along the radius. Denote by g(x) the value of the negative logarithm of the x-ray at fixed axial distance, at a distance x from the axis Denote by f(r) the value of the product $\rho\mu$ at distance r from the axis. Then

$$g(x) = 2 \int_x^a \frac{rf(r)dr}{\sqrt{r^2 - r_x^2}} . \qquad (3)$$

where a is some radius beyond which f(r) vanishes. We have measured g(x) and can calculate numerically the value of f(r).

The two radiographs were digitized on a PDS scanning microdensitometer at 50 micron spacing with a 50 micron by 50 micron aperture; 512 lines with 1024 pixels per line were obtained. Figures 1 and 2 show the digitized radiographs.

These radiographs were then displayed on the Comtal 8000 digital image display and an interactive program was utilized to determine the centerline of the projectile. The maximum tilt of the projectile from ideally normal impact was measured and was less than 2^0. The needed projections were then extracted from the digitized radiograph.

To reduce film grain noise, a median or Tukey filter was used on each line. Figure 3a shows one line of the original input data of the 4.8 μs radiograph with film noise. This line is near the top of the projectile (about ten lines below the top). The median filter was applied to this line, its negative logarithm then taken and then corrected for the polychromatic source.

The x-ray absorption coefficient for this material in the range of the incident x-ray spectrum is essentially independent of x-ray energy;[3] therefore, this effect of beam hardening is small. The intensity outside the projectile image is nearly constant throughout this line and throughout the entire radiograph and was subtracted from the entire digitized projection. The resulting projection was then inverted numerically line by line to give the material density along that line (Fig. 3b).

Since the expected variation of density in a shock wave or rarefaction wave is of the order of 0.5%-10%, the images were enhanced by a linear stretch from 67.5% peak density to 100% peak density in eight grey level increments (Figs. 4 and 5). Each grey level represents a 1.56% relative density step in $\Delta\rho/\rho$. This enhancement brings out significant detail. In the 4.8 μs picture, a slightly curved shockwave is visible near the top of the projectile and a rarefaction wave is seen to extend from the intersection of the shockwave and the outer edge to the axis and then continues on from the axis (in the picture this looks as if the wave reflects from the axis). There is also an annular high compression zone whose center is at the intersection of the edge of the projectile and the plate. A fine resolution enhancement showed a

very narrow ridge of slightly higher density extending from the center recompression zone. Higher density regions appear behind the top shock and the reflected rarefaction. Densities in the spray are very low. The enhanced picture for the 11.2 μm radiograph shows no definable wavefronts, but shows a pronounced density structure. The recompression zone has shifted towards the axis. A different enhancement, concentrating on lower densities, shows a narrow crack extending from the center line and bounding the lower density bubble.

The density fields obtained from radiographs can be compared to those obtained from computer simulations and the adequacy of the assumed material response functions judged from the extent of agreement. A Lagrangian program (SALE), using artificial viscous pressure in the shock, gave the solutions shown in Fig. 6 and 7 for a simple fluid model in symmetric impact (677 m/s). In this calculation the pressure is given by the Mie-Gruneisen form referred to the shock Hugoniot, but modified to give negligible rupture strength.

The prominent features of the radiographs appear also in the simulation: the inital shock (21 kb) rapidly attenuated by lateral expansion, followed by jetting and a recompression to near the stagnation pressure (5 kb), beginning near the periphery and converging to the center, finally producing at the impact face a disc of warm material at normal density and, at the back face, a dome of spalled material at low density. Some details of the simulations are less plausible and would be regarded as numerical artifacts were they not present also in the resolved radiographs: the slightly higher density at the center of the impact face and the shell of normal density material rising from the compacted disc near the edge. The recompression is of particular interest in this system, because it has been proposed as a trigger for the delayed detonation often observed in propellants under these conditions.

TABLE I

COMPOSITION BY WEIGHT OF THE INERT POLYMER-BONDED EXPLOSIVE (PBX) MOCKUP CYLINDERS

Constituent	Wt.%
Cross linked polymers	19.00
Plasticizer	10.00
Powdered Aluminum (5 μm)	19.50
Talc	14.12
Salt (100 μm)	17.38
Salt (50 μm)	20.0

REFERENCES:

1. Kruger, R. P., G. W. Wecksung, and Morris, R. A., "Industrial Applications of Computed Tomography at Los Alamos National Laboratory" Optical Engineering, 19, 273-282, (1980).

2. Fugelso, E, "Material Density Measurements from Dynamic Test X-ray Radiographs Using Axisymmetric Tomography," Los Alamos Scientific Laboratory, LA-8785-MS (1981).

3. Seigbahn, K., ed. Alpha, Beta and Gamma Ray Spectroscopy, Vol. I, North Holland (1965).

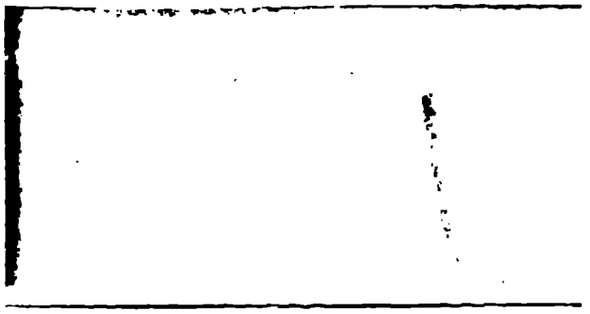

Fig. 1. Digitized radiographic of the mockup PBX cylinder striking a steel plate at 4.8 μsec after impact. Striking velocity is 677 m/sec.

Fig. 2. Digitized radiograph of the mockup PBX cylinder striking a steel plate at 11.2 μsec after impact. Striking velocity is 677 m/sec.

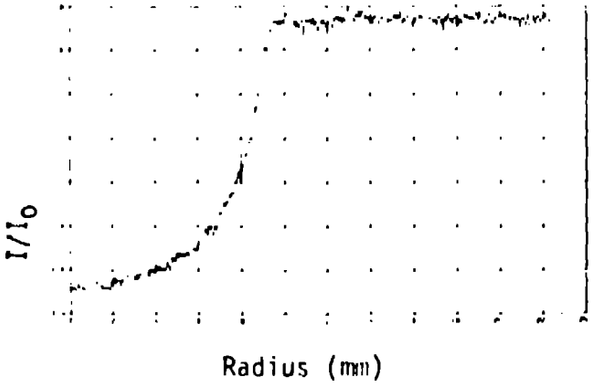

Fig. 3a. Radiographic film density versus radius for one line of the scanned data 1 mm from the top of the projectile. Time of radiograph is 4.8 μsec.

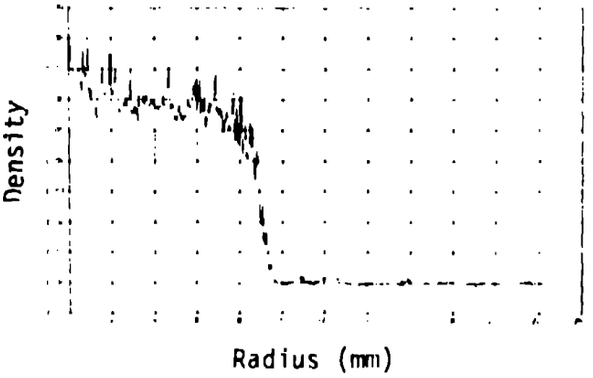

Fig. 3b. Reconstruction of the density profile as a function of radius.

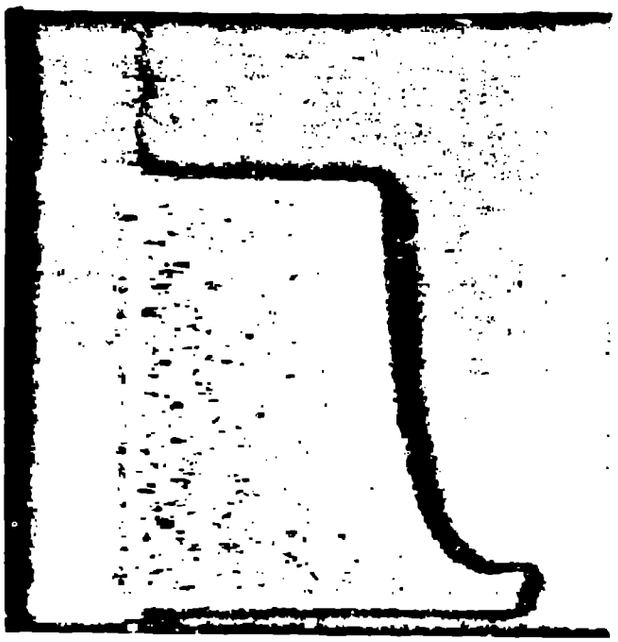

Fig. 4. Enhanced image (linear stretch) for the projectile at 4.8 μsec after impact. A shock wave and two rarefaction waves are now visible.

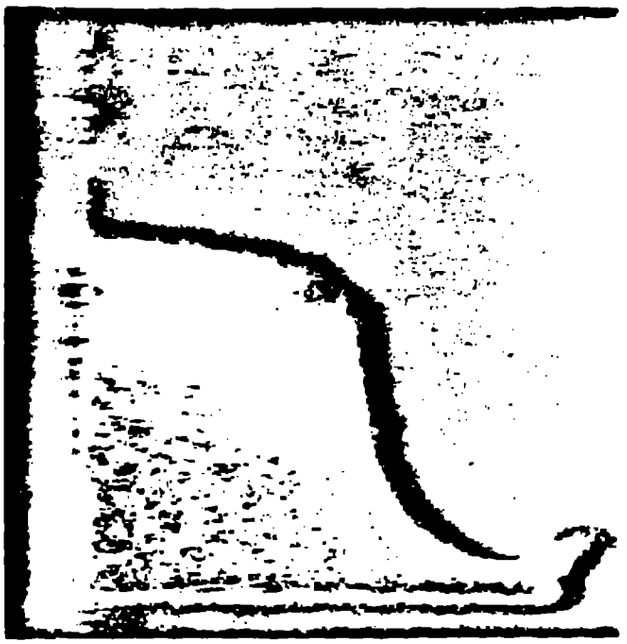

Fig. 5. Enhanced image (linear stretch) for the projectile at 11.2 μsec after impact. No specific wavefront structure is visible, but the density gradients are quite pronounced.

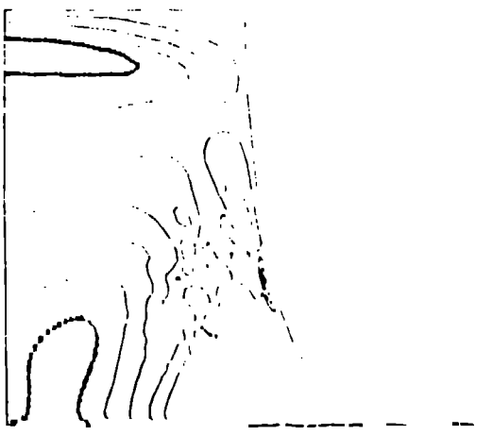

Fig. 6. Calculated density contours for impact of a mockup PBX cylinder striking a steel plate at 677 m/s at 6.0 ms after impact. Maximum and minimum density ratios are 1.140 and 0.815. Density contours are 0.033.

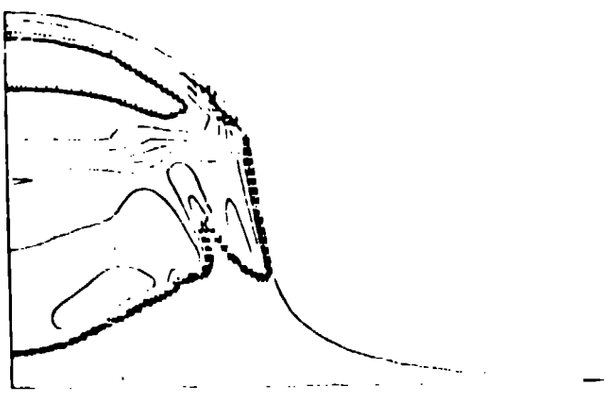

Fig. 7. Calculated density contours for impact of a mockup of PBX cylinder striking a steel plate at 677 m/s at 12.0 ms after impact. Maximum and minimum density ratios are 1.027 and 0.304. Density contours are .073.